JACC: CARDIOVASCULAR INTERVENTIONS VOL. 2, NO. 3, 2009

ISSN 1936-8798/09/$36.00
PUBLISHED BY ELSEVIER INC. DOI: 10.1016/j.jcin.2008.09.014

Antegrade Percutaneous Closure of Membranous Ventricular Septal Defect Using X-Ray Fused With Magnetic Resonance Imaging

Kanishka Ratnayaka, MD,*† Venkatesh K. Raman, MD, FACC,*
Anthony Z. Faranesh, PhD,* Merdim Sonmez, MS,*‡§ June-Hong Kim, MD,*
Luis F. Gutiérrez, PhD,* Cengizhan Ozturk, MD, PhD,*§ Elliot R. McVeigh, PhD,*
Michael C. Slack, MD, FACC,*† Robert J. Lederman, MD, FACC*

Bethesda, Maryland; Washington, DC; Princeton, New Jersey; and Istanbul, Turkey

Objectives We hypothesized that X-ray fused with magnetic resonance imaging (XFM) roadmaps might permit direct antegrade crossing and delivery of a ventricular septal defect (VSD) closure device and thereby reduce procedure time and radiation exposure.

Background Percutaneous device closure of membranous VSD is cumbersome and time-consuming. The procedure requires crossing the defect retrograde, snaring and exteriorizing a guidewire to form an arteriovenous loop, then delivering antegrade a sheath and closure device.

Methods Magnetic resonance imaging roadmaps of cardiac structures were obtained from miniature swine with spontaneous VSD and registered with live X-ray using external fiducial markers. We compared antegrade XFM-guided VSD crossing with conventional retrograde X-ray–guided crossing for repair.

Results Antegrade XFM crossing was successful in all animals. Compared with retrograde X-ray, antegrade XFM was associated with shorter time to crossing (167 ± 103 s vs. 284 ± 61 s; $p = 0.025$), shorter time to sheath delivery (71 ± 32 s vs. 366 ± 145 s; $p = 0.001$), shorter fluoroscopy time (158 ± 95 s vs. 390 ± 137 s; $p = 0.003$), and reduced radiation dose–area product (2,394 ± 1,522 mG·m^2 vs. 4,865 ± 1,759 mG·m^2; $p = 0.016$).

Conclusions XFM facilitates antegrade access to membranous VSD from the right ventricle in swine. The simplified procedure is faster and reduces radiation exposure compared with the conventional retrograde approach. (J Am Coll Cardiol Intv 2009;2:224–30) © 2009 by the American College of Cardiology Foundation

From the *Translational Medicine Branch, Division of Intramural Research, National Heart, Lung, and Blood Institute, National Institutes of Health, Bethesda, Maryland; †Cardiology Division, Children's National Medical Center, Washington, DC; ‡Siemens Corporate Research, Princeton, New Jersey; and the §Biomedical Engineering Institute, Bogazici University, Istanbul, Turkey.
This work was supported by the Division of Intramural Research, National Heart, Lung, and Blood Institute, National Institutes of Health (grant Z01-HL005062-04 CVB). AGA Medical Corporation provided Amplatzer membranous ventricular septal defect occluder devices and delivery systems. Merdim Sonmez was an employee of Siemens Corporate Research. Dr. Slack receives compensation as a physician training proctor for Amplatzer Medical Corporation. Siemens Corporate Research and National Heart, Lung, and Blood Institute have a collaborative research and development agreement for specific registration modules to be used in hybrid X-ray-magnetic resonance imaging systems.

Manuscript received September 5, 2008; accepted September 15, 2008.

Percutaneous closure of membranous ventricular septal defect (VSD) is now feasible using commercial devices (1,2). Conventional percutaneous techniques are cumbersome and require multiple steps—retrograde defect crossing, snare-recovery of a guidewire, formation of an arteriovenous guidewire loop, and placement of an antegrade delivery sheath—all before antegrade delivery of the occluder device (3). Moreover, sheath access may be lost during device delivery and the crossing steps must be repeated. The procedure is technically challenging, mainly because imaging limitations preclude direct antegrade access to the VSD from the right ventricle. As a result, conventional transcatheter VSD closure typically requires prolonged exposure to ionizing radiation.

To enhance image guidance, we combine magnetic resonance imaging (MRI) roadmaps with live X-ray (X-ray fused with magnetic resonance imaging [XFM]), based on external fiducial markers (4,5). We overlay MRI-derived features, such as VSD location and endoventricular contours, to position and deliver an asymmetric nitinol occluder device in swine.

We hypothesize that XFM enables direct antegrade crossing, simplifies and shortens procedure conduct, and reduces radiation exposure during closure in animals with congenital membranous VSD.

Methods

Animal procedures. Animal procedures were approved by the National Heart Lung and Blood Institute Animal Care and Use Committee. Fourteen Yucatan miniature swine (29 to 67 kg) with spontaneous VSD (Sinclair Research Center, Columbia, Missouri) were anesthetized with atropine, butorphanol, ketamine, and xylazine, and then maintained on isoflurane and mechanical ventilation. Four additional VSD miniswine were used during technical computer development and were not analyzed further.

Interventional procedures were conducted using percutaneous transfemoral artery and vein access. Left-to-right shunts were measured by oximetry and MRI. The VSD dimensions were measured using both MRI and radiocontrast angiography with calibrated catheters.

MRI and XFM registration. Experiments were conducted in a dual X-ray and MRI intervention suite (6). Sixteen fiducial markers conspicuous under both X-ray and MRI (Beekley Corp., Bristol, Connecticut), were secured on the thorax. End-expiratory roadmaps were obtained using MRI at 1.5-T (Espree, Siemens, Erlangen, Germany) and a standard 8-channel phased array surface coil. Typical electrocardiogram-gated segmented steady-state free precession (SSFP) acquisition parameters were: repetition time/echo time: 3/1.5 ms; flip angle: 80°; bandwidth: 930 Hz/pixel; 1.8 × 1.8 × 6 mm voxels. Typical "black-blood" turbo spin echo images used: repetition time/echo time: 700/34 ms; bandwidth: 292 Hz/pixel; 1.4 × 2.2 × 3 to 6 mm voxels. Typical phase-contrast gradient echo acquisition parameters were: repetition time/echo time: 6.3/2.9 ms; flip angle: 30°; bandwidth: 434 Hz/pixel; 1.4 × 2.5 × 6 mm voxels. The VSD dimensions were measured on representative long-axis SSFP and turbo spin echo MRI images.

After MRI, the animals were transferred to a single-plane X-ray system (Axiom Artis FC, Siemens) using a mechanized bidirectional transport table (Miyabe, Siemens). Single-phase MR images were registered to the live X-ray acquisitions (4). Briefly, external fiducial markers, conspicuous under both X-ray and MRI, were matched and the 2 coordinate systems were aligned with rigid-body registration algorithms using custom image processing software written in MATLAB (Mathworks, Cambridge, Massachusetts). The MRI regions of interest included contours of the VSD, ventricular cavities, outflow tracts, aortic valve, and aortic root (Fig. 1). These were segmented manually while the animals were transferred from MRI to X-ray and then presented to the operator as a static image overlay on real-time X-ray fluoroscopic images. Catheter procedures were conducted only in the X-ray lab.

Target registration error was defined as the 2-dimensional distance between VSD center-of-mass on X-ray cineangiography and SSFP MRI during systole at end-expiration. Although the defect could easily be visualized under MRI throughout the cardiac cycle, in cineangiography it was best identified by the jet of contrast ejected across the defect during systole.

Abbreviations and Acronyms

MRI = magnetic resonance imaging

SSFP = steady state free precession

XFM = X-ray fused with magnetic resonance imaging

VSD = ventricular septal defect

VSD closure procedures. DEFECT CROSSING: CONVENTIONAL, RETROGRADE TECHNIQUE. Figure 2A shows the standard crossing technique that we used (3). We first acquired a radiocontrast ventriculography roadmap in a cranial and left anterior oblique projection. We crossed the VSD using retrograde transaortic, braided 6-F coronary angiographic catheters from the left ventricle and positioned soft guidewires into a distal pulmonary artery branch. We captured and exteriorized the guidewire using a transfemoral venous snare (Amplatz Gooseneck, ev3 Inc., Plymouth, Minnesota) to form an arteriovenous loop.

To complete the procedure, a delivery sheath (Torqueview, AGA Medical, Plymouth, Minnesota) is advanced over this loop from the venous side across the VSD. We did not close the defects until techniques were compared.

DEFECT CROSSING: INVESTIGATIONAL, ANTEGRADE TECHNIQUE. We crossed antegrade using XFM from the right ventricle into the left ventricle using pre-formed diagnostic catheters and 0.035-inch hydrophilic guidewires (angled Glidewire, Terumo Medical Corporation, Somerset, New Jersey) (Fig. 2B).

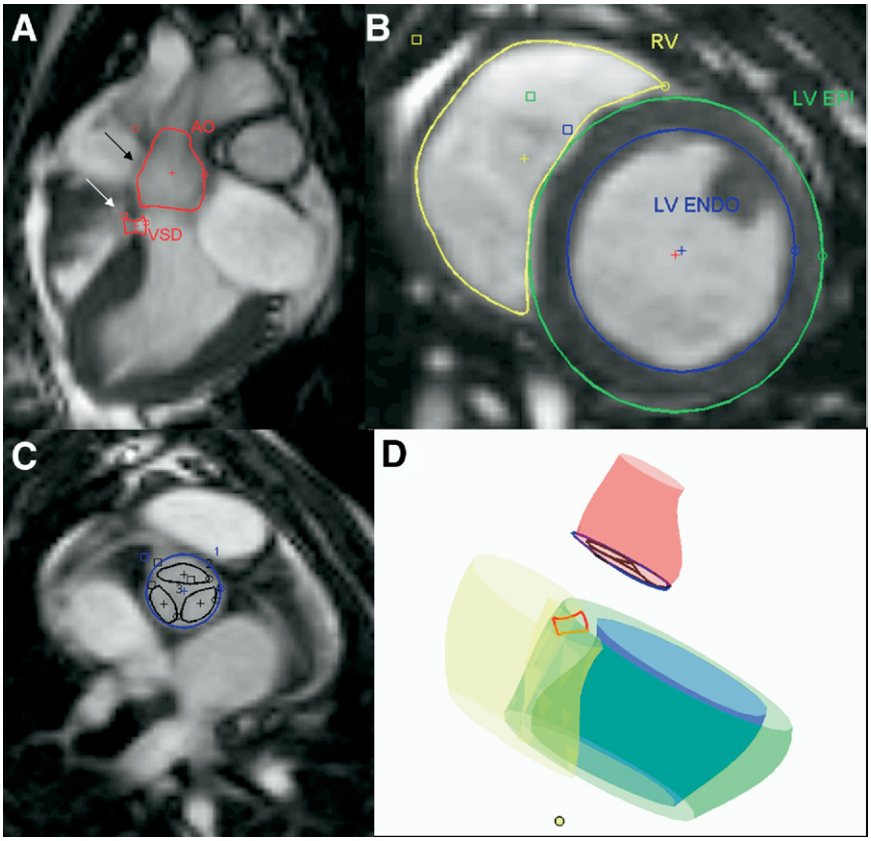

Figure 1. MRI-Derived Contours

(A) Long-axis 3-chamber SSFP MRI used to contour VSD **(white arrow)** and aortic root **(black arrow)**. **(B)** Short-axis SSFP MRI used to contour right **(yellow)** and left **(blue)** ventricular endocardial surfaces and left ventricular epicardial surface **(green)**. **(C)** Short-axis SSFP MRI used to contour aortic valve annulus **(blue)** and leaflets **(black)**. **(D)** Surface rendering of MRI-derived contours. The **yellow dot** indicates the left ventricular apex. See accompanying Online Video 3. AO = aorta; ENDO = endocardial surface; EPI = epicardial surface; LV = left ventricle; MRI = magnetic resonance imaging; SSFP = steady state free precession MRI; RV = right ventricle; VSD = ventricular septal defect.

Before closure, with the catheter in the descending aorta, the hydrophilic wire was exchanged for a rigid 0.035-inch guidewire (Supra-core, Abbott, Santa Clara, California).

PERCUTANEOUS MEMBRANOUS VSD DEVICE CLOSURE. The delivery sheath was advanced across the defect and into the descending aorta. Then the rigid wire was replaced with a flexible guidewire (Noodle, AGA Medical) to redirect the sheath toward the left ventricular apex.

The Amplatzer Membranous VSD Occluder was sized according to manufacturer instructions (1 to 2 mm larger than angiographic VSD diameter). The asymmetric left ventricular disk was oriented based on the XFM representation of the apex. Positioning was confirmed by radiocontrast ventriculography and aortography before device release and by MRI and necropsy afterward.

Experimental design. In an initial training phase (4 animals), we tested feasibility of XFM-guided antegrade VSD crossing.

In the experimental phase (10 animals), we recorded procedure times and radiation exposure. We tested each approach 3 to 4 times in each animal in random order (conventional retrograde followed by investigational antegrade or investigational followed by conventional). First, we compared antegrade VSD guidewire crossing under X-ray or XFM guidance using identical catheter technique (3 animals). Next, we compared antegrade XFM guidance with conventional retrograde X-ray guidance for VSD guidewire crossing and sheath delivery (7 animals). To preserve defect anatomy for crossing comparisons, relatively bulky (9-F) delivery sheaths were not advanced across the defect until all attempts were completed. Animals underwent cardiac MRI before euthanasia and necropsy. All procedures were performed by a single operator. To minimize "operator memory" effects, different image displays (monitors) were used for XFM-guided and conventional X-ray-guided procedures.

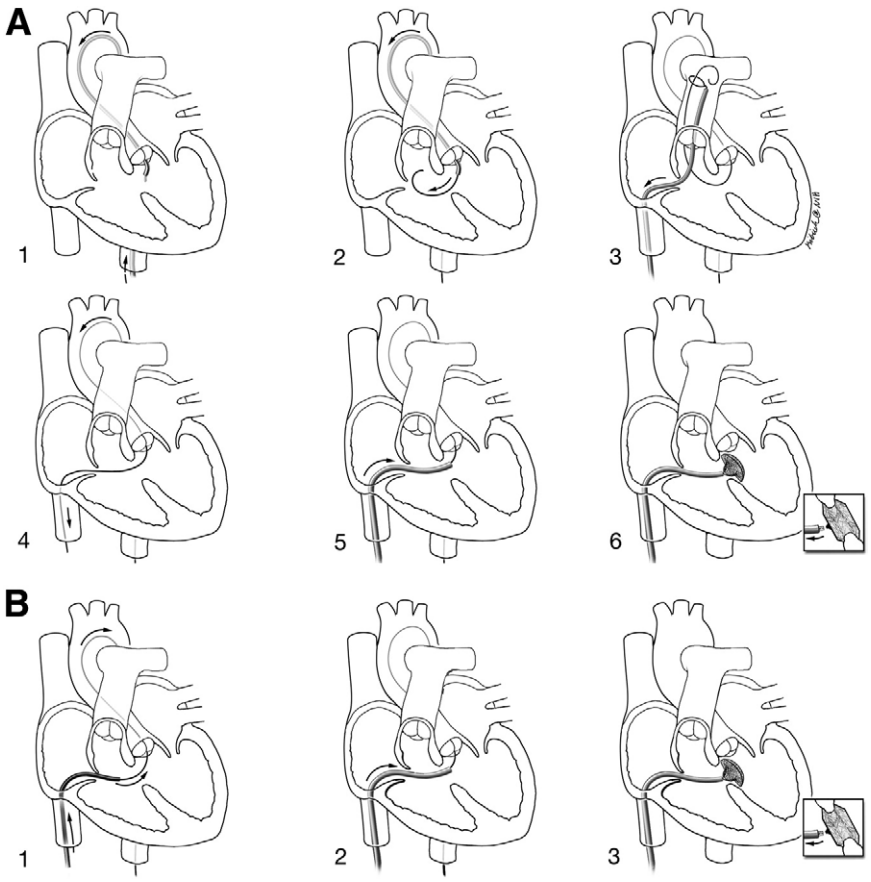

Figure 2. Schematic Depictions of Conventional and Investigational Procedure Technique

(A) Conventional retrograde X-ray technique. **(1)** Retrograde, transaortic access to the left ventricle. **(2)** A guidewire crosses retrograde from the left to right ventricle across the VSD. **(3)** A transfemoral venous snare retrieves the transaortic guidewire from the pulmonary artery. **(4)** An arteriovenous loop is exteriorized to provide a rail to deliver the rigid VSD delivery sheath. **(5)** The delivery sheath is positioned antegrade across the VSD. **(6)** The VSD occlusion device is positioned and released. **(B)** Investigational XFM-guided antegrade technique. **(1)** With enhanced imaging guidance, the guidewire is passed antegrade from the right ventricle through the VSD into the left ventricle and descending aorta. **(2)** The delivery sheath is positioned in the left ventricle. **(3)** The VSD occlusion device is positioned and released. The XFM technique has fewer steps. Courtesy of Lydia Kibiuk, NIH Medical Arts and Photography Branch. XFM = X-ray guided magnetic resonance imaging; other abbreviations as in Figure 1.

The *VSD crossing time* is defined as the time the femoral sheath is entered until the guidewire is in the distal pulmonary artery (retrograde) or descending aorta (antegrade). The *sheath delivery time* begins after the VSD is crossed and ends when the arteriovenous loop is formed (retrograde) or the descending aorta is entered with the rigid guidewire (antegrade). *Total fluoroscopy time* and *radiation exposure* encompass VSD crossing and sheath delivery.

Data analysis. For each animal we averaged 3 to 4 measurements, so as not to exaggerate the statistical degrees of freedom. Results are expressed as mean ± SD. Component procedure times and radiation exposure were compared using 2-tailed Student *t* tests, adjusted for unequal variances when appropriate (Excel, Microsoft, Redmond, Washington). Results were considered to be statistically significant at a value of $p < 0.05$.

Results

Anatomic and physiologic findings. Congenital membranous VSDs were evident on MRI and radiocontrast ventriculography. Defect diameter ranged from 2.5 to 8 mm. Pulmonary-systemic flow ratios ranged from 1.3 to 3.4 and were similar by oximetry and velocity-encoded MRI. Older animals tended to have smaller VSDs and aneurysmal tricuspid tissue encroaching on the VSD.

Procedural details and complications. In these experiments, 21 additional fluoroscopy frames were performed solely for registration with MRI, adding a total of 0.030 $mG \cdot m^2$ incremental radiation, or <1% of the total average radiation exposure for animal.

During technical development, we found that pre-formed catheters with right-handed 3-dimensional curves (Wil-

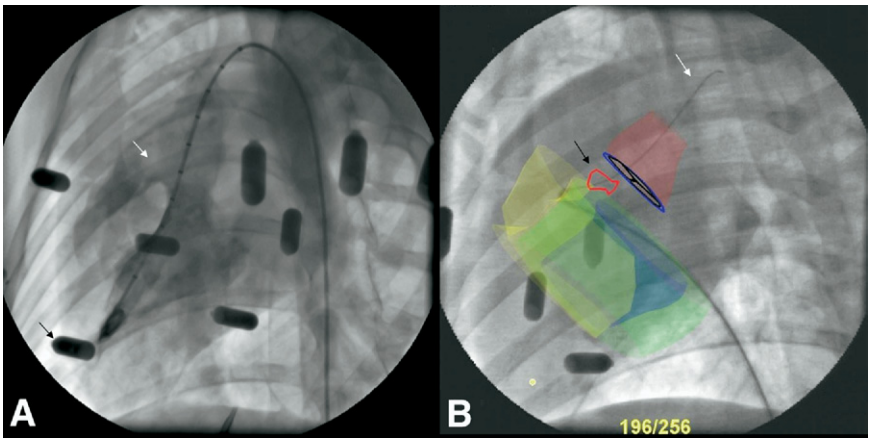

Figure 3. X-Ray Fluoroscopic Landmarks Compared With XFM Roadmaps

(A) X-ray depicts the ventricular septal defect **(white arrow)** only during radiocontrast injections. **Black arrows** indicate the external fiducial beads. **(B)** A representative image of direct antegrade VSD guidewire crossing using XFM guidance. The XFM roadmap elements include the right ventricular endocardial contour **(yellow)**, the left ventricular epicardial contour **(green)**, the left ventricular endocardial contour **(blue)**, the VSD tract **(red outline and black arrow)**, aortic root **(red)**, and aortic valve **(blue annulus with black leaflets)**. The guidewire **(white arrow)** is delivered across the VSD and into the aorta using a right-handed 3-dimensional curve right coronary artery catheter. The MRI-derived contours adjust automatically when the X-ray system is repositioned. See accompanying Online Video 1. Abbreviations as in Figures 1 and 2.

liams Right, 6-F Expo, Boston Scientific, Natick, Massachusetts) simplified antegrade crossing compared with single-plane curve shapes (Judkins right, right coronary bypass). We used Williams Right shaped catheters thereafter for antegrade crossing in the experimental phase.

The XFM registration was unavailable in 4 additional technical development experiments because of computer malfunction. In these, all VSD crossing attempts were unsuccessful despite 15 min of fluoroscopy and the procedures were aborted.

There were no procedural complications including conduction or rhythm abnormalities, atrioventricular or semilunar valvular regurgitation, or pericardial effusion. Moreover there was no sheath kinking or device embolization.

Comparison of image-guidance techniques. Antegrade XFM-guided crossing was successful in all 14 animals attempted (Online Video 1). Figure 3 demonstrates the utility of an MRI roadmap to provide a target for antegrade VSD crossing compared with X-ray alone. The system automatically updated MRI roadmaps "in real time" when table position, X-ray gantry angulation, magnification, and X-ray source image distance were changed. This was helpful, for example, to confirm guidewire, sheath, and device position.

We found that "blind" antegrade X-ray crossing generally required positioning the catheter near the expected VSD location and probing using a guidewire. By comparison, XFM generally permitted direct entry into the VSD with the catheter.

Compared with retrograde X-ray, antegrade XFM was associated with shorter time to crossing, shorter time to sheath delivery, shorter fluoroscopy time, and reduced radiation dose-area product (Table 1, Fig. 4A).

Likewise, XFM-guided antegrade VSD crossing was 5-fold faster than X-ray guided antegrade technique (itself not a conventional standard; XFM 69 ± 43 s vs. antegrade X-ray 366 ± 179 s; $p = 0.049$).

The XFM-guided device closure of VSD appropriately attenuated left-to-right flow across the defect without encroaching on the aortic valve leaflets (Fig. 4B, Online Video 2). Whether XFM or conventional X-ray technique was used first did not affect procedural time or radiation exposure.

Target registration error. Target registration error between center points on cineangiography and SSFP MRI derived VSD contours was 4.9 ± 2.3 mm.

Necropsy. Explanted hearts from 5 successive animals indicated appropriate device positioning, appropriate device angular orientation relative to the aortic valve, no encroach-

Table 1. A Comparison of Antegrade XFM With Conventional Retrograde X-Ray Guided Transcatheter VSD Repair

	Antegrade XFM	Conventional Retrograde X-Ray	p Value
VSD crossing, s	167 ± 103	284 ± 61	0.025
Sheath positioning, s	71 ± 32	366 ± 145	0.001
Total fluoroscopy, s	158 ± 95	390 ± 137	0.003
Radiation dose–area product, mG·m^2	2,394 ± 1,522	4,865 ± 1,759	0.016

VSD = ventricular septal defect; XFM = X-ray fused with magnetic resonance imaging.

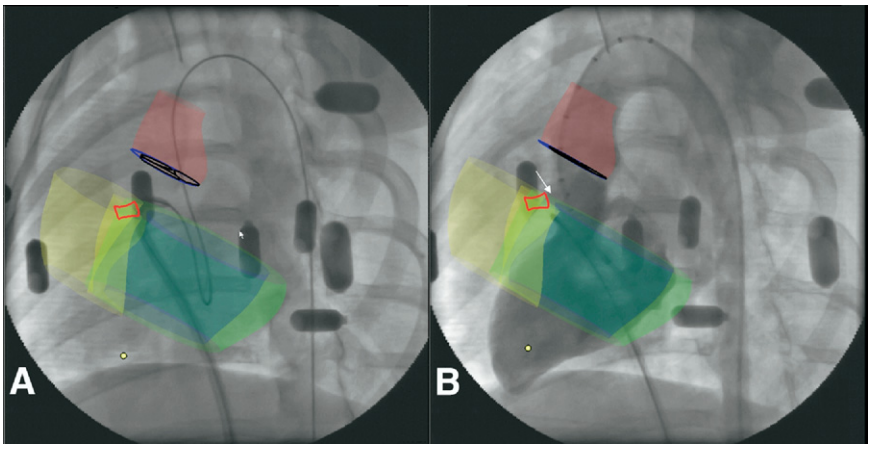

Figure 4. XFM Positioning of Delivery Sheath and VSD Occluder Deployment

(A) Antegrade sheath delivery guided by XFM. The sheath is directed toward the left ventricular apex using a flexible guidewire. The XFM roadmap includes right **(yellow)** and left **(blue)** ventricular endocardial contours, left ventricular epicardial contour **(green)**, aortic annulus **(blue)**, aortic root **(red)**, and VSD tract **(bright red)**. **(B)** Confirmatory XFM radiocontrast ventriculography before release of VSD occluder device deployed in position. Features include the VSD occluder **(white arrow)**, VSD tract **(bright red contour)**, right **(yellow)** and left **(blue)** ventricular endocardial and left ventricular epicardial **(green)** contours, aortic valve **(dark blue)**, and aortic root **(dark red)**. See accompanying Online Video 2. Abbreviations as in Figures 1 and 2.

ment on aortic valve leaflets, and freedom from tricuspid valve entrapment.

Discussion

Transcatheter closure of membranous VSD is technically challenging (7), primarily because contemporary interventional imaging tools delineate anatomy poorly. Fluoroscopy affords no landmarks to navigate across the VSD. As a result, direct antegrade access to the VSD is generally avoided. In this experiment, XFM enhances image guidance sufficiently to enable direct antegrade crossing and repair. It reduces the number of procedure steps, reduces procedure times, fluoroscopy, and radiation exposure. XFM continuously depicts the relationship between structures and their X-ray projection despite changes in gantry angulation and table position (Online Video 3). The XFM roadmaps also enhance subjective operator confidence by delineating critical intracardiac structures and spatial relationships.

Conventional versus antegrade repair. Right ventricular trabeculation (8), aneurysmal tricuspid valve tissue (9), and related flow perturbations interfere with antegrade percutaneous VSD crossing and closure. XFM mitigates these anatomic and functional obstacles. The VSD target displayed on XFM permits the operator to avoid chordal and trabecular entrapment. XFM allowed the operator directly to enter the VSD with the catheter. Conventional X-ray generally required the operator to find the VSD with a probing guidewire in a process that might entrap chordae.

XFM simplifies VSD closure into a direct antegrade procedure. By contrast, the conventional retrograde approach requires cumbersome crossing from left to right, snaring and then exteriorizing the guidewire to form an arteriovenous loop, followed by positioning and delivering the closure device under fluoroscopic and echocardiographic guidance.

Faster crossing and sheath delivery is particularly helpful during procedures complicated by inadvertent loss of sheath position, in which case these steps must be repeated. Direct antegrade crossing may also be germane to treatment of muscular and post-infarction VSD where defects are often multiple (10). That said, direct retrograde repair of muscular VSD has been reported (11).

Safety. Ionizing radiation is associated with a spectrum of malignancy (12). Children are especially sensitive to radiation exposure and may survive longer to experience radiation-associated toxicity. Children with congenital cardiovascular disease often require multiple exposures to medical radiation. Andreassi et al. (13) found evidence of chromosomal damage in patients with congenital heart disease exposed to radiation. The U.S. National Research Council considers cancer risk proportional to exposure even at the lowest levels (14). In this study, XFM halved radiation exposure.

Safe percutaneous VSD closure requires particular attention to critical structures such as the aortic valve (15). Subjectively, detailed soft tissue information from MRI enhances operator confidence navigating the complex spatial relationships among vital intracardiac structures. Indeed, when XFM was technically unavailable, our antegrade approach was not readily accomplished. XFM also facilitated appropriate orientation of the asymmetric occluder device with regard to the aortic valve

JACC: CARDIOVASCULAR INTERVENTIONS, VOL. 2, NO. 3, 2009
MARCH 2009:224–30

and cardiac apex, although we offer no quantitative supporting data.

Study limitations. We did not use transesophageal echocardiography or biplane fluoroscopy, which are typical adjuncts to conventional retrograde VSD repair. In our clinical experience, transesophageal and intracardiac echocardiography have value in selecting, positioning, and assessing closure devices, but have limited value in actual defect crossing, the procedure tested here. Biplane fluoroscopy might be expected to shorten retrograde crossing times slightly at the expense of additional radiation exposure. We did not compare XFM with newer 3-dimensional surface or transesophageal echocardiography (16). Three-dimensional target registration error is expected to be greater than the 2-dimensional measurements we report. These experiments were conducted in swine with congenital VSD and surrounding aneurysmal tricuspid valve tissue; humans have similar anatomy (17).

Future steps. We measured a target registration error of 4.9 ± 2.3 mm without correction for cardiac and respiratory motion. With further technical development, XFM systems might compensate for respiratory motion; automatically prepare multiphase MRI roadmaps for electrocardiography-synchronized overlay; register based on intrinsic fiducial landmarks rather than external beads; and incorporate additional imaging modalities such as ultrasound. That said, early generation XFM has been tested in humans (5,18) and is now suitable for clinical application in treatment of membranous and single or multiple muscular VSDs. Clinical end points might include technical success and morbidity, radiation exposure, and long-term outcomes.

Conclusions

The XFM procedure enhances the familiar X-ray environment with superior MRI soft tissue information to facilitate complex interventions. In this study, XFM simplified and shortened the procedure and reduced radiation exposure. Many congenital structural anomalies, with similarly complex intracardiac 3-dimensional anatomical spatial relationships, might also benefit from such fusion image guidance.

Acknowledgments

The authors thank Pat Russo, John Oslund, and Kurt Amplatz of AGA Medical Corp for providing Amplatzer membranous VSD occluder devices and delivery systems and Victor J. Wright, William H. Schenke, Joni Taylor, and Katherine Lucas for technical assistance.

Reprint requests and correspondence: Dr. Robert J. Lederman, Translational Medicine Branch, Division of Intramural Research, National Heart, Lung, and Blood Institute, National Institutes of Health, Building 10, Room 2c713, MSC1538, Bethesda, Maryland 20892-1538. E-mail: ledermar@nhlbi.nih.gov.

REFERENCES

1. Minette MS, Sahn DJ. Ventricular septal defects. Circulation 2006; 114:2190–7.
2. Carminati M, Butera G, Chessa M, et al. Transcatheter closure of congenital ventricular septal defects: results of the European Registry. Eur Heart J 2007;28:2361–8.
3. Mullins CE. Cardiac Catheterization in Congenital Heart Disease: Pediatric and Adult. Malden, MA: Blackwell Futura, 2006.
4. de Silva R, Gutierrez LF, Raval AN, McVeigh ER, Ozturk C, Lederman RJ. X-ray fused with magnetic resonance imaging (XFM) to target endomyocardial injections: validation in a swine model of myocardial infarction. Circulation 2006;114:2342–50.
5. Gutierrez LF, Silva R, Ozturk C, et al. Technology preview: X-ray fused with magnetic resonance during invasive cardiovascular procedures. Catheter Cardiovasc Interv 2007;70:773–82.
6. Dick AJ, Raman VK, Raval AN, et al. Invasive human magnetic resonance imaging: feasibility during revascularization in a combined XMR suite. Catheter Cardiovasc Interv 2005;64:265–74.
7. Butera G, Chessa M, Carminati M. Percutaneous closure of ventricular septal defects. State of the art. J Cardiovasc Med (Hagerstown) 2007;8:39–45.
8. Lock JE, Block PC, McKay RG, Baim DS, Keane JF. Transcatheter closure of ventricular septal defects. Circulation 1988;78:361–8.
9. Carminati M, Butera G, Chessa M, Drago M, Negura D, Piazza L. Transcatheter closure of congenital ventricular septal defect with Amplatzer septal occluders. Am J Cardiol 2005;96:52L–8L.
10. Holzer R, Balzer D, Cao QL, Lock K, Hijazi ZM. Device closure of muscular ventricular septal defects using the Amplatzer muscular ventricular septal defect occluder: immediate and mid-term results of a U.S. registry. J Am Coll Cardiol 2004;43:1257–63.
11. Jameel AA, Arfi AM, Arif H, Amjad K, Omar GM. Retrograde approach for device closure of muscular ventricular septal defects in children and adolescents, using the Amplatzer muscular ventricular septal defect occluder. Pediatr Cardiol 2006;27:720–8.
12. Kleinerman RA. Cancer risks following diagnostic and therapeutic radiation exposure in children. Pediatr Radiol 2006;36 Suppl 14:121–5.
13. Andreassi MG, Ait-Ali L, Botto N, Manfredi S, Mottola G, Picano E. Cardiac catheterization and long-term chromosomal damage in children with congenital heart disease. Eur Heart J 2006;27:2703–8.
14. National Research Council (U.S.). Committee to Assess Health Risks from Exposure to Low Level of Ionizing Radiation. Health Risks From Exposure to Low Levels of Ionizing Radiation: BEIR VII Phase 2. Washington, DC: National Academies Press, 2006.
15. Fu YC, Bass J, Amin Z, et al. Transcatheter closure of perimembranous ventricular septal defects using the new Amplatzer membranous VSD occluder: results of the U.S. phase I trial. J Am Coll Cardiol 2006;47:319–25.
16. Acar P, Abadir S, Aggoun Y. Transcatheter closure of perimembranous ventricular septal defects with Amplatzer occluder assessed by real-time three-dimensional echocardiography. Eur J Echocardiogr 2007;8: 110–5.
17. Ho SY, Thompson RP, Gibbs SR, Swindle MM, Anderson RH. Ventricular septal defects in a family of Yucatan miniature pigs. Int J Cardiol 1991;33:419–25.
18. Rhode KS, Sermesant M, Brogan D, et al. A system for real-time XMR guided cardiovascular intervention. IEEE Trans Med Imaging 2005;24:1428–40.

Key Words: image-guided intervention ■ interventional magnetic resonance imaging ■ congenital heart disease ■ multimodality image fusion ■ heart septal defects ■ ventricular.

APPENDIX

For supplementary videos and their legends, please see the online version of this article.